

Glacial meltwater and primary production are drivers of strong CO₂ uptake in fjord and coastal waters adjacent to the Greenland Ice Sheet

L. Meire^{1,2,3}, D. H. Sogaard¹, J. Mortensen¹, F. J. R. Meysman^{2,4}, K. Soetaert², K. E. Arendt¹, T. Juul-Pedersen¹, M. E. Blicher¹, and S. Rysgaard^{1,5,6,7}

¹Greenland Institute of Natural Resources, Greenland Climate Research Centre, P.O. Box 570, Kivioq 5, 3900 Nuuk, Greenland

²Royal Netherlands Institute of Sea Research (NIOZ), Department of Ecosystem Studies, Koringaweg 7, 4401, Yerseke, the Netherlands

³University of Ghent (UGent), Marine Biology Laboratory, Krijgslaan 281 (S8), 9000 Gent, Belgium

⁴Department of Analytical, Environmental and Geochemistry, Vrije Universiteit Brussel (VUB), Pleinlaan 2, 1050 Brussel, Belgium

⁵Centre for Earth Observation Science, Department of environment and Geography, University of Manitoba, Winnipeg, MB R3T 2N2, Canada

⁶Department of Geological Sciences, University of Manitoba, Winnipeg, MB R3T 2N2, Canada

⁷Arctic Research Centre, Aarhus University, 8000 Aarhus, Denmark

Correspondence to: L. Meire (lorenz.meire@ugent.be)

Abstract

The Greenland Ice Sheet releases large amounts of freshwater, which strongly influences the physical and chemical properties of the adjacent fjord systems and continental shelves. Glacial meltwater input is predicted to strongly increase in the future, but the impact of meltwater on the carbonate dynamics of these productive coastal systems remains largely unquantified. Here we present seasonal observations of the carbonate system over the year 2013 in the surface waters of a west Greenland fjord (Godthåbsfjord) influenced by tidewater outlet glaciers. Our data reveal that the surface layer of the entire fjord and adjacent continental shelf are undersaturated in CO_2 throughout the year. The average annual CO_2 uptake within the fjord is estimated to be $65 \text{ g C m}^{-2} \text{ yr}^{-1}$ indicating that the fjord system is a strong sink for CO_2 . The largest CO_2 uptake occurs in the inner fjord near to the Ice Sheet and high glacial meltwater input during summer months correlates strongly with low $p\text{CO}_2$ values. This strong CO_2 uptake can be explained by the thermodynamic effect on the surface water $p\text{CO}_2$ resulting from the mixing of fresh glacial meltwater and ambient saline fjord water, which results in a CO_2 uptake of 1.8 mg C per kg of glacial ice melted. We estimated that 28 % of this CO_2 uptake can be attributed to the input of glacial meltwater, while the remaining part is due to high primary production. Our findings imply that glacial meltwater is an important driver for undersaturation in CO_2 in fjord and coastal waters adjacent to large Ice Sheets.

1 Introduction

The Arctic Ocean plays an important role in the global carbon cycle and contributes 5–14 % to the global ocean CO_2 uptake (Bates and Mathis, 2009). High biological productivity combined with high seasonality in freshwater input and sea ice cover lead to strong dynamics in the carbonate system (Kaltin and Anderson, 2005). Increasing water temperatures, freshwater input and decreasing ice cover will likely have a profound effect on [the carbon cycle of the coastal Arctic Ocean](#) and will likely amplify the large seasonal and spatial biogeochemi-

cal gradients that occur in this area (Bates and Mathis, 2009; Mathis et al., 2011). While 25 % of the global continental shelves (water depth <200 m) are located in the Arctic, we still have a limited understanding of the carbon dynamics in these high-latitude coastal systems due to the scarcity of studies compared to low latitude coastal environments (Bates and Mathis, 2009). As a result, there are many open questions on how the carbon cycle in the Arctic will be affected by future environmental changes.

Many of the coastal systems in the Arctic are affected by glacial meltwater input, which leaves a unique biogeochemical fingerprint upon their surface waters (Etherington et al., 2007; Bamber et al., 2012; Raiswell 2013). Up to now only a few studies have investigated the CO₂ uptake in Arctic fjord systems impacted by glacial meltwater input (Evans et al., 2013; Rysgaard et al., 2012; Sejr et al., 2011). All these studies report substantial CO₂ undersaturation in the surface water. Data from a seasonal study in the mouth of Godthåbsfjord (SW Greenland) revealed low CO₂ partial pressure of ($p\text{CO}_2$) in the surface water thus leading to high CO₂ uptake rates from the atmosphere (83 to 108 g C m⁻² yr⁻¹). As yet a lot of uncertainty remains on the drivers of this high carbon sink (Rysgaard et al., 2012). On the one hand, high primary production estimates in West Greenland waters (67 to 500 g C m⁻² yr⁻¹; Jensen et al., 1999; Juul-Pedersen et al., 2014; Rysgaard et al., 2012) indicate that biological processes may have a strong effect on the carbonate dynamics and CO₂ uptake. On the other hand, the hypothesis has been put forward by Rysgaard et al. (2012) that glacial meltwater may exert a strong impact on the CO₂ dynamics of Arctic fjord systems. However, the relative importance of biology versus glacial meltwater input is presently uncertain nor are the mechanisms clear of how glacial meltwater input can stimulate CO₂ uptake.

Accelerated mass loss from the Greenland Ice Sheet and rapid climate change (Rignot et al., 2011) demand a conceptual understanding of how different drivers affect the carbon cycle in high latitude coastal areas. The main focus of this study is to investigate the mechanisms controlling the CO₂ uptake in fjord systems and shelf areas affected by glacial meltwater by means of a case study in the Godthåbsfjord (Greenland). To this end, an extensive sampling program was set up in 2013 involving monthly sampling at three dedi-

cated stations in the fjord, in addition to seasonal transects across the whole fjord and shelf system. Data covering the full annual cycle of partial pressure of CO₂, dissolved inorganic carbon (DIC) and total alkalinity (TA) were collected alongside hydrographic and biological parameters. This approach allowed us to resolve the seasonal importance of the different drivers in CO₂ uptake and the impact of glacial meltwater on the carbonate dynamics in these high-latitude coastal systems.

2 Material and methods

2.1 Field site

This study was conducted in the Godthåbsfjord system (Nuup Kangerlua, southwest Greenland), which covers an area of 2013 km² and has a volume of 525 km³ (Fig. 1). The mean depth of the fjord is 260 m and there is a sill of 170 m depth located at the entrance of the fjord (Mortensen et al., 2011; Rysgaard et al., 2012). Six outlet glaciers drain into the fjord system. Recent hydrological simulations estimate the annual freshwater input to Godthåbsfjord (excluding solid ice discharge as well as submarine melt from glaciers) to be $22.5 \pm 5.2 \text{ km}^3 \text{ yr}^{-1}$ for the period 1991–2012 (Langen et al., 2014). Ice sheet runoff accounts for 60 % of the freshwater input, land runoff is responsible for 34 %, and net precipitation over the fjord surface represents the remaining 6 % (Langen et al., 2014). Van As et al. (2014) project a similar estimate of 10–20 km³ glacial ice loss per year (solid ice discharge, surface ice melt and submarine melt) for the Godthåbsfjord glaciers.

2.2 Data

Data was collected during four cruises in 2013 (February, May, August and September/October) along a length-transect of 20 stations which covered the entire fjord as well as the Fyllas Banke, the adjacent part of the West Greenland continental shelf (Fig. 1). The dataset was further complemented by monthly sampling at three selected stations GF3, GF7 and GF10 over the period from May 2012 to December 2013. These 3 sampling sta-

tions are representative for 3 different zones in the fjord (Fig. 1). Zone 1 (with GF3 as representative station) comprises the outer part of the fjord (referred to as outer sill region by Mortensen et al., 2011), which is characterized by strong tidal currents, deep mixing and a weak summer stratification. Zone 2 (represented by GF7) covers the central part of the fjord, which is characterized by a relatively deep mixed stratified layer. Finally zone 3 (with GF10 as representative) is the inner part close to the freshwater sources, which is most strongly affected by glacial meltwater and experiences strong salinity stratification.

At each station and sampling time, conductivity and temperature depth profiles were recorded by a CTD instrument (Seabird SBE19plus), which was equipped with a fluorescence (Seapoint Chlorophyll Fluorometer) and Photosynthetic Active Radiation sensor (LI-COR 190SA quantum Q PAR sensor). Partial pressure of carbon dioxide ($p\text{CO}_2$) was measured in situ using the HydroC™ Carbon Dioxide Sensor (Contros, Germany) at seven water depths (1, 5, 10, 20, 30, 40 and 50 m). At every depth the HydroC sensor was equilibrated for 2–5 min until a stable reading was obtained. [The HydroC sensor was serviced and calibrated yearly by the Contros company. The relative standard deviation \(RSD\) of the \$p\text{CO}_2\$ measurement has been estimated to be 1 % \(Fietzek et al., 2014\).](#)

Water samples were collected at eight water depths (1, 5, 10, 20, 30, 40, 100 and 400 m) using 5 liter Niskin bottles (KC Denmark Research Equipment). Unfiltered water was transferred by gastight Tygon tubing to 12.5 mL exetainers (Labco, UK) for dissolved inorganic carbon (DIC) and total alkalinity (TA) analysis. Exetainers were left to overflow and samples were preserved by adding 0.02 % of a saturated HgCl_2 solution (Dickson and Goyet, 1992). Samples were stored in darkness at 4 °C until further analysis. DIC was measured using an infra-red DIC analyzer (Apollo SciTech), which consists of an acidification and purging unit in combination with a LI-COR-7000 $\text{CO}_2/\text{H}_2\text{O}$ Gas analyser. The RSD for DIC were ± 0.1 % ($n = 10$). TA was determined using the standard operating procedure for open cell potentiometric titration (Dickson et al., 2007, SOP 3b), using an automatic titrator (Metrohm 888 Titrand), a high accuracy burette (1 ± 0.001 mL), a thermostated reaction vessel ($T = 25$ °C) and combination pH glass electrode (Metrohm 6.0259.100). TA values were calculated by a non-linear least-squares fit to the titration data (Dickson et al., 2007,

SOP 3b) in a custom-made script in the open source programming framework R (R Core Team, 2013). The RSD of the procedure was $\pm 0.2\%$ ($n = 10$). Quality assurance of TA and DIC analysis involved regular analysis of Certified Reference Materials (CRM Batch 126 provided by A. G. Dickson, Scripps Institution of Oceanography). [As noted by Bates et al. \(2014\), no CRM are presently available for samples at low salinities and low alkalinities, and so the assumption is made that quality assurance based on CRM remains robust at low salinities.](#)

Water samples for chlorophyll analysis were filtered through 25 mm GF/F filters (Whatman, nominal pore size of $0.7 \mu\text{m}$). Filters were placed in 10 mL of 96 % ethanol for 18 to 24 h and chlorophyll fluorescence in the filtrate was analyzed using a fluorometer (TD-700, Turner Designs) before and after addition of 200 μL of a 1 M HCl solution.

Primary production was measured using the ^{14}C incubation method (Nielsen, 1952). Incubation bottles were filled with 55 mL unfiltered seawater and spiked with 175 μL $\text{NaH}^{14}\text{CO}_3$ ($20 \mu\text{Ci mL}^{-1}$) and incubated for two hours in an ICES incubator (Hydro-Bios, Germany). The samples were filtered onto 25 mm GF/F filters (Whatman) and 100 μL of 1 M HCl was added to remove excess $\text{NaH}^{14}\text{CO}_3$ and the filters were left open for 24 h in the fume hood. Subsequently, 10 mL of scintillation cocktail (Ultima Gold, Perkin Elmer) was added to the samples before counting them on the scintillation counter (Liquid Scintillation Analyzer, Tri-Carb 2800TR, PerkinElmer). After subtracting fixation rates obtained from the dark incubations, gross primary production rates were calculated based on measured DIC concentrations. Photosynthesis-Irradiance (P-I) curves were obtained for 11 sampling dates at 2 separate depths (5 and 20 m). The light extinction coefficient was calculated from the measured PAR profile. Solar irradiance values were obtained from the meteorological survey in Nuuk (Meteorological station 522, Asiaq Greenland Survey). Using the solar irradiance at each day, the light extinction coefficient and the P-I curves at the monthly sampling dates, the daily productivity was calculated over the entire year. This approach assumes that light extinction and P-I curves remain the same in the two-week period before and after the sampling dates.

Bacterial production was measured using the ^3H -thymidine method (Fuhrman and Azam, 1982). **Triplicate samples (10 mL) were incubated at in situ temperature in the dark.** After an incubation of 6 to 8 h, bacterial activity incubations were stopped by adding 500 μL of 100 % trichloroacetic acid (TCA). The samples were subsequently filtered through 25 mm cellulose ester filters (pore size 0.2 μm , Advantec MSF). The equations from Sogaard et al. (2010) were used to calculate bacterial production. For the calculation of the bacterial carbon demand from the bacterial production, a bacterial growth efficiency of 0.5 was used according to Rivkin et al. (2001).

The difference in $p\text{CO}_2$ between surface water and atmosphere drives the air–sea CO_2 exchange (ASE), which was calculated using the relation:

$$\text{ASE} = K_{\text{av}}\alpha\Delta p\text{CO}_2 \quad (1)$$

where $\Delta p\text{CO}_2$ is the difference in $p\text{CO}_2$ of the surface water (here at 1 m water depth) and the atmospheric $p\text{CO}_2$. Negative values of ASE imply an uptake by the surface seawater and positive values an efflux to the atmosphere. The atmospheric $p\text{CO}_2$ was measured monthly at GF3 using an infrared CO_2 monitor (EGM-4 PP systems). The mean atmospheric $p\text{CO}_2$ was 400 μatm for 2013. The quantity α is the solubility of CO_2 in seawater ($\text{mol m}^{-3} \text{atm}^{-1}$). K_{av} (m s^{-1}) is the gas transfer coefficient calculated using both the formulation of Nightingale et al. (2000) and Wanninkhof and McGillis (1999). These formulations depend on the wind speed data (m s^{-1}) at 10 m a.s.l., obtained from a weather station located in the fjord system (Meteorological station 522, Asiaq Greenland Survey). The monthly mean wind speed varied from 5 to 9 m s^{-1} for 2012 and 2013 but during storms peak wind speeds up to 30 m s^{-1} were recorded.

Processing of data was done in the open-source programming language R (R Core Team, 2013). The R package CRAN: AquaEnv (Hofmann et al., 2010) was used for acid-base speciation and CO_2 system calculations. **We used the carbonate equilibrium constants by Roy et al. (1993) with the adaptation by Millero et al. (1995) for low salinities. Consequently the dissociation constants are valid over a salinity range of 0–45 and temperature range from 0–45 °C. To test the sensitivity of our calculations we also implemented the equilibrium**

constants by Millero et al. (2006), which had a negligible impact, thus showing that our thermodynamic calculations of the CO₂ system are robust against the choice of the carbonate equilibrium constants. Interpolation of the data and contour plots were produced using the R package CRAN: Akima (Akima et al., 2006).

2.3 Biogeochemical model

To analyze the impact of the glacial meltwater input on the seasonal carbon dynamics of the fjord system, a simplified biogeochemical model was constructed. The model describes how the $p\text{CO}_2$ dynamics in the surface water is influenced by the circulation in the fjord, the input of glacial meltwater, air–sea exchange of CO₂ and net ecosystem production. This biogeochemical model is constrained by an inverse modelling procedure using the monthly data from the 3 reference stations as well as the data from the four seasonal transects across the fjord system.

The biogeochemical model of the fjord system is composed out of three separate, connected boxes, representing the outer, central and inner part of the fjord system and one large “open sea” box, representing the outer shelf; the latter was added to obtain full mass balance closure. Each box represents the upper 40 m of the water column since this depth range is most strongly affected by primary production (due to light availability) and the glacial meltwater imprint (via stratification). The model includes a water mass balance in addition to the mass balances of three state variables (salinity, DIC and TA) for each box (Table 1). Once DIC and TA are known, all relevant parameters of the carbonate system (including $p\text{CO}_2$) can be calculated.

2.3.1 Water mass balance

Figure 2 shows a simplified circulation model for the fjord system. Intrusion of coastal water into the fjord, leads to deep water upwelling and an input of saline water (F_i) in each of the three zones. The inner zone of the fjord experiences an input of glacial meltwater (Q_g). The combination of saline seawater intrusion and freshwater from the glacier results in a return

flow (Q_i) in the surface water which is eventually discharged onto the Greenland shelf. The resulting water mass balance equations are shown in Table 1 (Eqs. 1–3, Table 1). Based on these water balance equations, a subsequent mass balance for salinity can be constructed in the three different zones (Table 1).

The magnitude of the different water flows in the fjord system is unknown and these flows are expected to vary strongly throughout the year due to the strong seasonality in the glacial meltwater input as well as seasonal inflows of coastal water (Mortensen et al., 2011). The water mass balance provides 3 independent equations, which allows to constrain the three return flows, $Q_i(t)$, when the seawater inputs, $F_i(t)$, and glacial meltwater input, $Q_g(t)$, are known.

The variation of the glacial meltwater input with time, $Q_g(t)$, was estimated from salinity observations at station GF10 close to the outlet glaciers. The total annual meltwater input into Godthåbsfjord was constrained to be $20 \text{ km}^3 \text{ yr}^{-1}$ as derived from regional climate model simulations for Godthåbsfjord (Langen et al., 2014; Van As et al., 2014). The relative contribution of freshwater (x) at station GF10 was estimated from a two end-member mixing model ($S = x \cdot S_{\text{FW}} + (1 - x) \cdot S_{\text{SW}}$) (Sect. 2.3.3.). The contribution x was calculated at each month and fitted with a smoothing spline. Assuming that x scales with $Q_g(t)$, the temporal variation of x was used to predict the temporal variation of Q_g , ensuring that integrated annual meltwater was equal to $20 \text{ km}^3 \text{ yr}^{-1}$.

The values of the three remaining seawater inputs ($F_i(t)$) in the different zones were obtained by an inverse modelling approach using the monthly salinity data obtained at the three representative stations (GF3, GF7 and GF10). To this end, we estimated the salinity changes dS_i/dt in the different zones by fitting a cubic smoothing spline (Hastie and Tibshirani, 1990) through the monthly salinity data and subsequently taking the derivative. If we implement both the observed salinities and the salinity changes, we obtain a linear set of three equations (Eqs. 4–6, Table 1), which allows to estimate the seawater inputs ($F_i(t)$).

2.3.2 Dissolved inorganic carbon balance

The different water flows as derived from the water and salinity mass balances were used to parameterize the transport terms in the mass balances for TA (Eqs. 7–9, Table 1) and DIC (Eqs. 10–12, Table 1). Alkalinity was assumed to behave conservatively within the fjord, and hence was only influenced by transport (Thomas and Schneider, 1999). In contrast, the DIC mass balance accounted for transport processes, but also air–sea exchange of CO₂ (ASE) and net community production (NCP) (Table 1). Air–sea CO₂ fluxes were calculated according to Eq. (1) using the formulation by Nightingale et al. (2000) for the gas transfer coefficient. The *p*CO₂ concentration of the surface water was calculated from salinity, temperature, TA and DIC using the R package CRAN: AquaEnv (Hofmann et al., 2010). The net community production (NCP) was calculated as the difference between the primary production (PP) and bacterial carbon demand (BCD) and values for the rate of these processes were determined based on monthly rate measurements. Accordingly, NCP was imposed as a forcing function upon the model.

2.3.3 End members composition

The model uses two end-member types of water as input, freshwater (FW) from glacial meltwater and saline water (SW) intruding across the sill and upwelling from the deeper fjord to the surface layer. The composition (S, DIC, TA) of both end-member types of water was determined based on collected data. As detailed above, the largest fraction of the freshwater input (60%) is from glacial origin and so we used the properties of glacial meltwater for the freshwater end-member. To this end, twenty samples were collected from icebergs in the fjord. Salinity, DIC and TA were measured after thawing the ice in the laboratory in gas-tights bags ($S_{FW} = 0$, $DIC_{FW} = 80 \pm 17 \mu\text{mol kg}^{-1}$, $TA_{FW} = 50 \pm 20 \mu\text{mol kg}^{-1}$). As noted above, the Godthåbsfjord is also affected by other freshwater sources: 34% originates as surface runoff from the surrounding watershed, while 6% is attributed to direct precipitation on the water surface of the fjord system (Langen et al., 2014). Samples collected from snow indicate an average DIC concentration in snow of $74 \mu\text{mol kg}^{-1}$ (Søgaard, unpublished data; TA was

not measured). This value lies close to the values measured in ice samples, and indicates that surface runoff could be similar to the glacier meltwater. Accordingly, we prefer the use of the most parsimonious model, which only considers one type of freshwater end-member, for which we used the measured properties of the glacial meltwater. However, characteristics of freshwater are likely characterized by similar properties (low DIC and low TA) compared to the seawater end-member. For the seawater end-member, we used the properties of deep fjord water (water at 400 m depth) which is shown to be comparable to the properties of the water on the shelf ($S_{\text{SW}} = 33.65$, $\text{DIC}_{\text{SW}} = 2150 \mu\text{mol kg}^{-1}$, $\text{TA}_{\text{SW}} = 2220 \mu\text{mol kg}^{-1}$ and $T_{\text{SW}} = 2^\circ\text{C}$). The properties of SW end-member were assumed not to vary through the year. The bottom water DIC and TA in the deep part of the fjord shows little seasonality, as the fjord is relatively deep (up to 600 m), and this large volume buffers against fluctuations induced by remineralization of organic matter originating from plankton blooms.

2.3.4 Numerical solution

A numerical solution procedure for the resulting differential equations was implemented in the open-source programming language R following Soetaert and Meysman (2012). The set of differential equations was integrated using the R package CRAN: deSolve (Soetaert et al., 2010). The calculation of the carbonate system (and hence $p\text{CO}_2$) at each time step of the numerical simulation was performed via the operator splitting approach as detailed in Hofmann et al. (2008). The resulting $p\text{CO}_2$ concentration then can be employed in the kinetic rate expression for the air–sea CO_2 exchange. The model was run over a full seasonal cycle (representing the year 2013) and with a spin-up period of 2 years. The goodness of fit (GOF) between model simulation output and observational data was calculated as the sum of squared residuals.

3 Results

3.1 Carbon dynamics in the Godthåbsfjord fjord system

The hydrography of Godthåbsfjord is strongly affected by the seasonal input of glacial meltwater. Figure 3 shows the spatial distribution of salinity in the upper 40 m of the water column during four cruises in 2013 (February, May, August and October). The length transect ranges from the Greenland continental shelf to the inner part of the fjord where six glaciers discharge. Low freshwater runoff during winter and spring months coincides with high salinities ~ 33 in the upper 40 m of the water column throughout the fjord (Fig. 3a and b). Increased input of glacial meltwater during summer creates a strongly stratified system, where the surface water shows a distinct layer in the central and inner part of the fjord (Fig. 3c). Due to distribution of freshwater sources, the impact is most pronounced at the inner fjord stations (GF9 to GF13), where in August salinity drops to ~ 8 in a shallow surface water layer of 10 m depth. In the central fjord (GF5 to GF8), summer salinity decreases to 17 and the upper layer of low-saline water layer extends deeper to 15–20 m depth. In the outer part of the fjord (the outer sill region, GF1 to GF4) the salinity decrease with depth is less pronounced as the freshwater is mixed deeper into the water column by strong tidal mixing. Still, even at the shelf stations (FB1 to FB4), a weak imprint of glacial meltwater can be observed. Decreased input of glacial meltwater during the autumn months coincides with a gradual increase in salinity in the surface layer and a less steep halocline (Fig. 3d).

Strong seasonality was also observed in the fluorescence data (Fig. 4). Evidence of a spring bloom is indicated by the high chlorophyll *a* concentrations on the shelf (FB4 to FB1) and in the central fjord (GF5 to GF8) observed during the May cruise (Fig. 4b). In contrast to the May situation, where the chlorophyll *a* is evenly distributed in the upper 40 m of the water column, distinct chlorophyll maxima were observed in August (Fig. 4c). During the August cruise, high fluorescence values of $\sim 6 \mu\text{g L}^{-1}$ were observed at the outer shelf stations at approximately 30 m depth (FB4 and FB3.5). Clear chlorophyll *a* maxima also occurred in the central and inner part fjord with values of $\sim 10 \mu\text{g L}^{-1}$ at 20 m depth at GF8 and values of $\sim 15 \mu\text{g L}^{-1}$ at 10 m depth in the inner fjord (GF9 to GF12). In February

and October low chlorophyll *a* concentrations were measured throughout the entire fjord and shelf system (all values lower than $1 \mu\text{g L}^{-1}$; note that values are missing for the shelf region in February).

Surface waters were permanently undersaturated in CO_2 with respect to atmospheric equilibrium in the surface waters of the entire fjord system throughout the whole year 2013 (note that only surface $p\text{CO}_2$ data is available for February). Maximum $p\text{CO}_2$ surface values of $\sim 350 \mu\text{atm}$ were measured in February, and at this time, surface $p\text{CO}_2$ did not vary throughout the fjord (Fig. 5a). In May CO_2 undersaturation became more pronounced, and the lowest values were observed over the shelf and in the surface layer at the inner fjord stations (Fig. 5a). At the shelf stations, low $p\text{CO}_2$ values ($< 240 \mu\text{atm}$) were observed throughout the water column and these coincided with DIC concentrations lower than $2000 \mu\text{mol kg}^{-1}$ that were also homogeneous throughout the water column (Figs. 5b and 6a). Despite the occurrence of low $p\text{CO}_2$ values ($\sim 200 \mu\text{atm}$) coinciding with low DIC ($\sim 1950 \mu\text{mol kg}^{-1}$) in the surface layer of the inner fjord stations, high $p\text{CO}_2$ values ($> 300 \mu\text{atm}$) and high DIC concentrations ($> 2000 \mu\text{mol kg}^{-1}$) were observed in the layer below 20 m depth (Figs. 5b and 6a).

In August a further decrease in surface $p\text{CO}_2$ was observed in the central and inner part of the fjord (Fig. 5c). Undersaturation was strongest at stations closest to the tidewater outlet glaciers where $p\text{CO}_2$ values as low as $74 \mu\text{atm}$ were measured (Fig. 5c). At this time, the DIC concentration also dropped below $800 \mu\text{mol kg}^{-1}$ in the upper meters of the water column (Fig. 6b). Below this shallow layer of low-saline water, DIC concentrations and $p\text{CO}_2$ values increased strongly with depth, reaching respectively $\sim 2000 \mu\text{mol kg}^{-1}$ and $\sim 330 \mu\text{atm}$ at 40 m depth. The water layer depleted in $p\text{CO}_2$ and DIC extends to greater depth in the central region of the fjord (GF5-GF8, Figs. 5c and 6d) but the undersaturation in the surface is not as pronounced compared to the stations close to the tidewater glaciers. For the stations on the shelf, the $p\text{CO}_2$ values in August were similar to those observed in May (Fig. 5a) though a subsurface minimum with $p\text{CO}_2$ values lower than $220 \mu\text{atm}$ was observed at 30 m depth at one of the slope stations (FB3.5, Fig. 5c).

In October $p\text{CO}_2$ and DIC values in the surface waters gradually increased again compared to the previous campaigns (Figs. 5a and 6c). The lowest values were still found in the inner part of the fjord (Figs. 5d and 6c). Gradients with depth were not as strong, most likely due to reduced stratification (Fig. 3d).

3.2 CO_2 dynamics close to the glaciers

Time series from the station GF10, located in the inner fjord system (Fig. 1), show the seasonal evolution in the depth-averaged values (0–40 m) for salinity and temperature (Fig. 7a), the parameters of the carbonate system (Fig. 7b), chlorophyll *a* (Fig. 7c) and primary production and bacterial carbon demand (Fig. 7d). The mean salinity in the upper water column was ~ 33 during late winter and spring when freshwater runoff to the fjord is at its minimum (Fig. 7a). Around early June, salinity started to decrease rapidly and attained its annual minimum (~ 27 in 2013) in August, corresponding to the period of highest freshwater input due to glacial melt. From August onwards to late winter, salinity showed a gradual increase after which values remained constant from March to June. Temperature ranged from 0.5 to 3.5 °C and showed a more irregular seasonal pattern. Lowest temperature was observed in February whereas the highest value was recorded in October. During the period from March to August 2013, the depth-averaged temperature fluctuated around 1.5 °C (Fig. 7a).

The seasonal cycle of the carbonate system tracked the temporal evolution of salinity. Values of $p\text{CO}_2$, DIC and TA showed a gradual increase during the winter months in the upper 40 m. Maximum values were obtained in March with depth-averaged values of $p\text{CO}_2 \sim 350 \mu\text{atm}$, DIC $\sim 2040 \mu\text{mol kg}^{-1}$ and TA $\sim 2200 \mu\text{mol kg}^{-1}$. In April 2013, the $p\text{CO}_2$ dropped rapidly and reached $\sim 250 \mu\text{atm}$ by the mid of May, while the average DIC concentration in the upper 40 m simultaneously decreased to $\sim 1950 \mu\text{mol kg}^{-1}$ (Fig. 7b). Coinciding with this spring decrease in DIC and $p\text{CO}_2$, high chlorophyll *a* concentrations were observed (Fig. 7c). High primary production rates match the high chlorophyll *a* concentrations and also bacterial carbon demand increased (Fig. 7d). During the subsequent summer months, DIC in the upper 40 m decreased to an average concentration of $1850 \mu\text{mol kg}^{-1}$ in 2013 (and $\sim 1700 \mu\text{mol kg}^{-1}$ in 2012), coinciding with the strong salinity decrease due to

glacial meltwater runoff. The alkalinity shows a similar decrease in response to the increase in freshwater input. Despite the strong $p\text{CO}_2$ decrease in the upper 20 m, with concentrations down to $100 \mu\text{atm}$ in the surface water of the inner fjord (Fig. 5c), the summer decrease of $p\text{CO}_2$ at GF10 (Fig. 7b) was less pronounced (minimum at $\sim 200 \mu\text{atm}$) due to depth averaging (mean over 0–40 m layer). Continued primary production and bacterial carbon demand was observed after the spring bloom although rates are lower and depth averaged chlorophyll a values were around $2\text{--}3 \mu\text{g L}^{-1}$ (Fig. 7c and d). From October onwards, the $p\text{CO}_2$, TA and DIC concentrations started to increase slowly to reach the maximal winter values, while chlorophyll a values were negligible.

Measurements of primary production and bacterial carbon demand allowed to estimate net community production in station GF10, giving a value of $85 \text{ g C m}^{-2} \text{ yr}^{-1}$ for 2013.

3.3 Air–sea exchange of CO_2 in the fjord system

Using the monthly surface $p\text{CO}_2$ data collected at three stations (GF3, GF7 and GF10) over 2013, the air–sea CO_2 flux can be quantified using wind speed data from the meteorological station at Nuuk (Fig. 8a). $p\text{CO}_2$ in surface waters was permanently below atmospheric $p\text{CO}_2$ leading to a CO_2 uptake during the entire year (Fig. 8b). Depending on the formulation of the gas transfer coefficient (Nightingale et al., 2000; Wanninkhof and McGillis, 1999), the mean annual CO_2 uptake at the inner fjord station GF10 is 70 to $82 \text{ g C m}^{-2} \text{ yr}^{-1}$. The GF7 station in the central fjord showed an average uptake of 60 to $66 \text{ g C m}^{-2} \text{ yr}^{-1}$, while the uptake was 37 to $39 \text{ g C m}^{-2} \text{ yr}^{-1}$ at GF3 in the outer part of the fjord. Based on these estimates data from the three stations, the area-averaged annual CO_2 uptake in the entire fjord system was calculated to be $\sim 65 \text{ g C m}^{-2} \text{ yr}^{-1}$.

The mean CO_2 uptake was also calculated for the seasonal transects in May, August and October based on the measured $p\text{CO}_2$ surface data and using the daily wind speed values during the month that spans the sampling date (i.e. 14 day period before and after). Confirming the pattern observed at the three monitoring stations, the uptake is higher close to the glaciers and lower in stations downstream the fjord, but rises slightly again over the shelf (Fig. 8c). Lower surface $p\text{CO}_2$ in the central and inner fjord led to almost a doubling of

the CO₂ uptake in the inner part of the fjord compared to the outer part. The wind however plays also an important role: despite higher surface $p\text{CO}_2$ values in May, higher wind speed (Fig. 8a) led to a higher CO₂ uptake. Anova analysis indicates that uptake is significantly different between stations and between months ($P < 0.001$).

3.4 Model results: driving factors of the carbon dynamics

To resolve the importance of the different driving forces of CO₂ uptake in the fjord, a simplified biogeochemical model was used to simulate the DIC and $p\text{CO}_2$ in the region closest to the glacier (GF10, zone 3) (Fig. 2). This zone is most strongly affected by glacial meltwater input and primary production, and hence, shows the highest excursions in the parameters of the carbonate system. Figure 9 shows the simulated annual cycle of DIC and $p\text{CO}_2$ at GF10 compared with the measured data. Simulations were performed (1) with and without the effect of net community production on carbon dynamics and (2) with a constant temperature throughout the year (the average mean winter temperature in upper 40 m, which was 0.5 °C) or with a variable temperature based on the observations. Simulations that included NCP managed to reproduce the DIC and $p\text{CO}_2$ evolution better as quantified by goodness of fit. NCP has especially a strong effect on the evolution of the $p\text{CO}_2$. The inclusion of seasonal temperature variation had overall a moderate effect on the simulation output. Higher temperatures during summer and autumn (1.5 to 3 °C, Fig. 7a) led to a reduction of $p\text{CO}_2$ undersaturation in the simulation with variable temperature.

Figure 10 summarizes how transport processes (including the input of glacial meltwater), air–sea exchange and biological processes affected the change in DIC concentration in GF10. The DIC dynamics shows 3 distinct periods. From January to March, the net change in DIC is positive and DIC increased slowly to maximum values (Period I). DIC subsequently decreased strongly in April coinciding with high NCP (Period II). In July and August, a second decrease in DIC was observed (Period III) coinciding with strong input of glacial meltwater. From September onwards the DIC concentration started to increase again to its maximum winter values (Period I).

4 Discussion

4.1 Air–sea CO₂ exchange in fjord and coastal waters adjacent to the Greenland Ice Sheet

Our observations of low $p\text{CO}_2$ in the Godthåbsfjord fjord system in south Greenland complement the existing observations of sub-arctic nearshore and off-shore areas showing a marked CO₂ undersaturation. The surface waters of the shelf area (Fyllas Banke) and the Godthåbsfjord fjord were strongly undersaturated in CO₂ relative to the atmosphere during the entire year (Fig. 5), and this strong undersaturation led to a high uptake of CO₂. Based on our data from monthly measurements during 2012–2013 at 3 stations in the fjord, we calculated a mean annual CO₂ uptake of $65 \text{ g C m}^{-2} \text{ yr}^{-1}$. This estimate is lower than the uptake of 83 to $108 \text{ g C m}^{-2} \text{ yr}^{-1}$ estimated earlier for the outer sill region of Godthåbsfjord (Rysgaard et al., 2012). The difference between both estimates is possibly explained by strong interannual variability in the flux (Rysgaard et al., 2012). Our estimate for the CO₂ uptake in Godthåbsfjord is higher than values previously reported from other sites in Greenland, such as $52 \text{ g C m}^{-2} \text{ yr}^{-1}$ offshore in the Greenland sea (Nakaoka et al., 2006) and $32 \text{ g C m}^{-2} \text{ yr}^{-1}$ in Young Sound, a fjord in Northeast Greenland (Sejr et al., 2011), indicating that Godthåbsfjord is a strong sink of CO₂. Our estimates for the CO₂ uptake at the Fyllas Banke shelf area (0.15 to $0.6 \text{ g C m}^{-2} \text{ d}^{-1}$) are also substantially higher than the average uptake of $0.04 \text{ g C m}^{-2} \text{ d}^{-1}$ reported by Chen et al. (2013) for shelf areas located higher than 50° N . This underscores that the coast off southwest Greenland is an important sink for CO₂, and further corroborates the idea that high-latitude shelves in general are important CO₂ sinks.

4.2 Effect of glacial melt on the carbon dynamics

Our data shows the strongest undersaturation in CO₂ (Fig. 5a and c) and the highest CO₂ uptake in the inner part of the Godthåbsfjord system (Fig. 8). High CO₂ uptake has been reported before in fjord systems affected by glacial meltwater (Rysgaard et al., 2012; Sejr

et al., 2011; Torres et al., 2011) indicating that glacial melt could affect the carbonate dynamics and drive CO₂ uptake. However, the actual mechanism via which glacial melt induces such strong undersaturation in CO₂ has not been elucidated yet.

Glacial meltwater can affect undersaturation in different ways. First of all, the meltwater itself can be undersaturated in $p\text{CO}_2$. Iceberg samples collected in the Godthåbsfjord area showed an average DIC concentrations of $80 \pm 17 \mu\text{mol kg}^{-1}$ and TA of $50 \pm 20 \mu\text{mol kg}^{-1}$, yielding a $p\text{CO}_2$ value of $\sim 380 \mu\text{atm}$. Accordingly, the meltwater is slightly undersaturated compared to the measured atmospheric CO₂ values of $\sim 400 \mu\text{atm}$. Measurements by Sejr et al. (2011) in a meltwater river in east Greenland also indicated that meltwater is undersaturated in CO₂. Ryu and Jacobson (2012) however found CO₂ oversaturation in rivers between the Greenland Ice Sheet and the Kangerluusaq fjord that were fed by meltwater of land-terminating glaciers. However, by the time the water reached the actual fjord, the excess CO₂ had evaded and the river water was in equilibrium with the atmosphere. The low endmember values of glacial meltwater are further confirmed by linear regression of TA and DIC versus salinity of all our carbonate system observations (TA = $159 + 63^*S$; R squared 0.95 and DIC = $61 + 59^*S$; R squared 0.92). These relations are similar to those obtained by Rysgaard et al. (2012) (TA = $161 + 61^*S$ and DIC = $169 + 55^*S$), apart from the DIC value of the fresh water endmember. However, it should be noted that the freshwater endmember values derived from these relations should be interpreted with caution, as confidence intervals widen near the end points of the range covered by linear regression, which is aggravated by the scarcity of data points at low salinities. As a result, a large uncertainty propagates into the estimated DIC and TA values of the freshwater endmember. Therefore, we use here in further calculations the DIC and TA values based on our measurements of meltwater from iceberg samples. Input of glacial ice and subsequent melting will consequently create a CO₂ sink in Godthåbsfjord. Using a undersaturation in CO₂ of $\sim 380 \mu\text{atm}$ and a glacial freshwater discharge of $20 \text{ km}^{-3} \text{ yr}^{-1}$ to the fjord system (Langen et al., 2014; Van As et al., 2014), this directly translates into an uptake of $0.5\text{--}2.0 \text{ g C m}^{-2} \text{ yr}^{-1}$ in the Godthåbsfjord. This direct effect of glacial meltwater on $p\text{CO}_2$ undersaturation hence only

accounts for a minor fraction of CO₂ uptake in the fjord system (i.e., 1–3 % of the annual CO₂ uptake estimated to be 65 g C m⁻² yr⁻¹).

A second mechanism via which glacial meltwater can induce undersaturation in *p*CO₂ is the non-conservative behavior of *p*CO₂ during the mixing of fresh water and saline water. This mixing effect potentially explains a large part of the low *p*CO₂ (and consequent CO₂ sink) that we observed in the Greenland fjord systems. The mechanism can be understood by considering the mixing of two water parcels with different composition. When mixing is conservative, the concentration of a chemical compound obeys the relation

$$[E]_{\text{Mix}}(M_1 + M_2) = [E]_1M_1 + [E]_2M_2 \quad (2)$$

where $[E]$ is the concentration of the compound E and M are the masses of the water parcels. Salinity, TA and DIC are conservative quantities with respect to mixing (Wolf-Gladrow et al., 2007). However, the fact that TA and DIC mix conservatively, does not imply that *p*CO₂ will behave conservatively upon mixing. In other words, if two water parcels mix that are initially in equilibrium with the atmosphere, this does not imply that the resulting mixture will also be in equilibrium with the atmosphere. In fact, mixing of fresh water and saline water induces a strong *p*CO₂ undersaturation. Figure 11a shows the undersaturation created when two water masses at equilibrium are mixed, one with low salinity, low TA and low DIC (representative for melt water from glacial origin) and one with high salinity, high TA and high DIC (representative for saline fjord water). The mixture of these two parcels will be undersaturated in *p*CO₂ due to the thermodynamic effect of salinity on *p*CO₂. Consequently this water parcel will take up CO₂ when in contact with the atmosphere (Fig. 11a). Note that the strongest undersaturation is obtained when the resulting mixture has a salinity of ~ 8 and that undersaturation in CO₂ can exceed 200 μatm below the atmospheric level (Fig. 11a). [This salinity effect on pH and *p*CO₂ dynamics has been described previously for estuarine systems \(Mook and Koene, 1975; Whitfield and Turner, 1986\) and sea-ice \(Delille et al., 2007\) but as yet, the mechanism has not been invoked to explain the low *p*CO₂ in high latitude fjords and shelves.](#) In fjord systems affected by glacial melt, meltwater (with low TA, DIC and salinity) mixes with ambient fjord waters (with high TA, DIC and

salinity). This mechanism hence could constitute an important driver for undersaturation in CO_2 when large amounts of meltwater are discharged into the fjord, so that salinity levels are sufficiently reduced. The undersaturation in CO_2 that has been previously observed in other high latitude systems (Evans et al., 2014; Sejr et al., 2011; Torres et al., 2011) could possibly be explained by this same mechanism, since these systems also show the signature of a large input of glacial meltwater, leading to a strong reduction in salinity.

In Godthåbsfjord, undersaturation in CO_2 is strongest during the summer months when large volumes of meltwater are mixed with fjord water and salinity in surface layer drops to ~ 8 (which coincides with the maximum undersaturation observed in Fig. 11a). The correlation in the timing of $p\text{CO}_2$ undersaturation and meltwater discharge suggests that the salinity effect described above could be an important driver of the observed undersaturation in CO_2 . To verify this hypothesis, we used the salinity depth profiles recorded in August 2013 at the three monitoring stations. We calculated the associated $p\text{CO}_2$ depth profile, assuming that only the salinity effect is playing and that no other processes (such as air–sea exchange and NCP) are affecting the $p\text{CO}_2$ depth profile (Fig. 11b). In the upper meters of the water column close to the glacier, where large volumes of fresh water are discharged (Zone 2 and 3), a strong undersaturation effect is observed where $p\text{CO}_2$ values drop below $200 \mu\text{atm}$ (Fig. 11b). This indicates that glacier melt water input is indeed an important driver for the strong undersaturation in CO_2 and high CO_2 uptake as observed in summer in the inner part of Godthåbsfjord.

When freshwater is transported downstream, this water will gradually mix with larger quantities of saline seawater, and so its salinity will increase. Along this trajectory, a water parcel can accumulate more and more carbon due to air–sea CO_2 exchange. When using the freshwater and saline endmembers introduced above (Fig. 11), and employing standard thermodynamic calculations of the carbonate system, we calculated that for every kilogram of ice melted, a total amount of 1.8 mg C can be sequestered as CO_2 from the atmosphere, before the water exits the fjord at a salinity of 32. If we combine this with the estimated glacial melt input of $20 \pm 5 \text{ km}^3 \text{ yr}^{-1}$ (Van As et al., 2014), this mechanism could be responsible for an uptake of $18 \pm 5 \text{ g C m}^{-2} \text{ yr}^{-1}$ in the Godthåbsfjord system, which

constitutes 28 ± 7 % of the total CO_2 uptake by the fjord system. Our detailed model simulations using the hydrological model for the fjord system (Table 1), which explicitly accounts for spatial and temporal variability in the CO_2 uptake from the atmosphere, provide estimates in the range of $10 - 20 \text{ g C m}^{-2} \text{ yr}^{-1}$. Note however that the biogeochemical model assumes homogenized conditions over the 40 m water depth, and so it may underestimate the undersaturation in CO_2 in the upper water layer (Fig. 11b), thus explaining the lower estimates as obtained by the thermodynamic calculations.

4.3 A seasonal cycle in a glacial meltwater affected fjord

In addition to the input of glacial meltwater, other driving forces are affecting the annual cycle of the carbonate system in Godthåbsfjord. The relative importance of driving forces differs across the seasonal cycle. Our data suggest three distinct phases in the annual cycle, which is represented by the scheme in Fig. 10.

4.3.1 Phase I: autumn and winter period

During autumn, glacier melting decreases and freshwater runoff to the fjord slowly diminishes (Figs. 3 and 7). Combined with dense coastal inflows to the fjord, this leads to a gradual salinity increase in the upper water layer and flushing of accumulated freshwater out of the Godthåbsfjord system (Fig. 7) (Mortensen et al., 2011, 2013). Weakening of the surface stratification combined with strong winter storms lead to a stronger mixing of the upper water layers. DIC and $p\text{CO}_2$ concentration increases slowly due to advection of water masses with high DIC and $p\text{CO}_2$ (upwelling of fjord deep water) and continued air–sea exchange to reach an average surface water $p\text{CO}_2$ of $\sim 350 \mu\text{atm}$ (Figs. 7, 8 and 10). The largest part of the Godthåbsfjord is free from sea ice throughout the year. Only in some of the inner stretches, sea ice is present during winter in some years. In the stations and transects sampled in this study, no sea-ice was present during the winter of 2012 and 2013. It has been shown previously that calcium carbonate precipitation takes place in the sea ice in Godthåbsfjord (Søgaard et al 2013). However due to the limited extent of sea ice in the

fjord, the influence of the sea ice melt on the Godthåbsfjord system is very low and therefore the effect of sea ice on the carbonate dynamics and biogeochemistry is not accounted for here.

4.3.2 Phase II: spring bloom

At the start of April, a strong spring bloom is observed in the inner part of the fjord, leading to high chlorophyll *a* concentrations, high net primary production and strong CO₂ uptake (Fig. 7). This high biological carbon uptake decreases the DIC and lowers the *p*CO₂ to 250 μatm in the surface waters of the inner fjord (GF10) by the middle of May (Figs. 7 and 10). The strong effect of primary production on the *p*CO₂ is observed in the entire fjord system in May (Figs. 4 and 5). Low surface water *p*CO₂ concentrations occur in almost the entire fjord system and on the shelf. During this period, the impact of the glacial meltwater on the fjord system is not pronounced, and the upper water column is still well mixed (Mortensen et al., 2011, 2013). Consequently low *p*CO₂ occur at nearly constant salinity and the undersaturation is almost homogenous in the water column. This matches with the evenly distribution of the fluorescence in the upper 40 m (Figs. 3–5). Only in the inner part of the fjord a clear gradient in *p*CO₂ with water depth can be observed. Continued inflow of dense water into the fjord system leads to upwelling in the inner part of the fjord, bringing up the deep water masses rich in DIC and *p*CO₂ (Figs. 3 and 5) (Mortensen et al., 2011).

The strong effect of biological processes on *p*CO₂ is illustrated in Fig. 9. In a model simulation without NCP, the large drop in *p*CO₂ concentrations observed in the spring and summer data is not reproduced. The high *p*CO₂ undersaturation in the spring is consequently linked to high biological activity (Bates and Mathis, 2009; Shadwick et al., 2011; Thomas and Schneider, 1999). Combined with the high primary production rates, high vertical fluxes of chlorophyll *a* from sediment traps are observed in the fjord at this time, indicating that a large fraction of the organic material produced in the upper water layers sinks to deeper waters (Rysgaard et al., 2012). Primary production is consequently able to counteract the large CO₂ air–sea influxes and to maintain low *p*CO₂ in surface water (Figs. 5 and 9b).

This creates an efficient biological pump through the spatial separation of production and mineralization (Sejr et al., 2014; Thomas et al., 2004).

4.3.3 Phase III: summer glacial melt

After the initial decrease in spring, surface water DIC decreases further during summer, coinciding with the increased input and mixing of glacial melt water into the fjord. At the start of summer (June), glacial meltwater runoff initiates the lowering of the salinity in the upper water layers (Figs. 3 and 7). This freshwater input induces stratification in the upper part of the water column of the inner and central fjord (Fig. 3). The high freshwater input ($\sim 20 \text{ km}^3 \text{ yr}^{-1}$) has not only a strong effect on fjord hydrography (Mortensen et al., 2011) but also strongly affects the chemistry in the fjord system (Rysgaard et al., 2012) and biology (Arendt et al., 2013). Mixing of glacial meltwater with fjord water strongly reduces the salinity of upper water layers (Figs. 3 and 7) while also DIC and TA are diluted in the upper water layers (Fig. 7). Coincident with this dilution of DIC and TA, a notable strengthening of the undersaturation in CO_2 in the upper water can be observed, as $p\text{CO}_2$ decreased further from 250 to $100 \mu\text{atm}$ in the upper meter (Fig. 5). This leads to very low $p\text{CO}_2$ in the inner part of the fjord, close to the outlet glaciers and consequently a strong uptake of CO_2 (Fig. 8). Our analysis shows that the non-linear thermodynamic effect of salinity on $p\text{CO}_2$, induced by the mixing of glacial meltwater with fjord water, plays an important role in this observed summer reduction of $p\text{CO}_2$ (Sect. 5.2). In a simulation without biology, a drop in $p\text{CO}_2$ in the upper meters of the surface waters is predicted (Fig. 9b). The water column is however highly stratified and despite the very low values in the upper water layer, higher $p\text{CO}_2$ values are observed at 40 m depth. Subglacial melt plumes, discharging at the grounding line of the glacier (or at other submarine levels), bring up deep water rich in DIC and $p\text{CO}_2$ close to the glacier. This creates a strongly stratified layer with freshwater on top and subglacial meltwater found below 10 m depth as described by Mortensen et al. (2013). The input of subglacial water consequently balances the strong decrease in the upper meters leading to no obvious changes in the mean (0–40 m) $p\text{CO}_2$ during summer period (Fig. 7).

In addition to the large effect of glacial meltwater input, primary production remains a strong driver on DIC and $p\text{CO}_2$ dynamics during summer. Continued high production maintains low $p\text{CO}_2$ on the continental shelf area. Also in the inner fjord continued biological activity (with significant blooms) can be observed (Figs. 4, 5, 7 and 10). The input of glacial meltwater strongly reduces the alkalinity in the upper water layers affecting the buffering of the system (Reisdorph and Mathis, 2014; Torres et al., 2011). Consequently the system becomes extra susceptible to $p\text{CO}_2$ changes. Due to the low buffering capacity, a similar production at lower salinity (and TA values) in the upper water layers has a much stronger effect on $p\text{CO}_2$ and hence even the lower level of primary production during summer can keep $p\text{CO}_2$ at their low levels. Consequently primary production keeps acting as a driving force for creating undersaturation in the fjord system even though mean chlorophyll is lower compared to the spring months (Fig. 7). Measurements of net community production estimate the strength of the biological carbon pump to be $85 \text{ g C m}^{-2} \text{ yr}^{-1}$ indicating that biological processes are the most important driver for carbon dynamics in the fjord responsible for 65–70% of the total CO_2 uptake by the fjord system. However part of the biological activity can potentially be associated with glacial processes due to the subglacial freshwater discharge. In addition to the upwelling of DIC rich water, subglacial freshwater discharge leads to a strong upwelling of nutrients fuelling continuous productivity during the summer in the inner part of the fjord. Consequently both glacial meltwater and primary production can be considered as crucial drivers for the CO_2 uptake in coastal areas affected by glacial meltwater.

Part of the low $p\text{CO}_2$ created by glacial meltwater and biological processes in the fjord is however compensated by higher temperatures in summer and autumn which reduce the CO_2 solubility in water, therefor counteracting the established undersaturation (Fig. 9) (Shadwick et al., 2011; Takahashi et al., 2002). Higher temperatures reduce $p\text{CO}_2$ up to $50 \mu\text{atm}$ (Fig. 9), reducing the CO_2 uptake with 10–20% compared to constant temperature simulation.

5 Summary and outlook

Our observations show that Godthåbsfjord is a strong sink for CO₂ due to high biological carbon uptake and undersaturation induced by the input of glacial meltwater. During winter, absence of significant glacial meltwater and biological consumption brings the fjord waters near equilibrium with the atmosphere due to air–sea exchange. A strong bloom during spring leads to a decrease in DIC and $p\text{CO}_2$ indicating the importance of biological processes. During summer, primary production continues to play a central role in the carbon dynamics. But the input and mixing of glacial melt water also plays a crucial role during the summer months. The non-linear effect of salinity on surface water $p\text{CO}_2$ from the mixing of glacial meltwater and saline fjord water creates a strong $p\text{CO}_2$ undersaturation and CO₂ uptake, a mechanism that was yet undescribed for glacial systems. **The meltwater effect alone results in the Godthåbsfjord in an uptake of $36 \times 10^9 \text{ g C yr}^{-1}$, while extrapolated to the Greenland Ice Sheet (using a ice discharge rate of $1000 \text{ km}^3 \text{ yr}^{-1}$ as cited in Bamber, 2012), this increases to $1822 \times 10^9 \text{ g C yr}^{-1}$.** The processes driving the DIC and $p\text{CO}_2$ dynamics in Godthåbsfjord most likely also apply for other fjord systems and coastal settings that are affected by glacier meltwater. Consequently coastal areas of Greenland and other glacier-influenced areas probably constitute a much larger sink compared to other coastal areas and play a more important role in the high-latitude carbon cycle. Increased melting is anticipated as a result of climate change and will likely accelerate processes affecting carbon dynamics; it will increase the freshwater volume mixing in fjord systems and consequently likely enhance the sink for CO₂ in fjord systems affected by glacial melt. **Finally, if the entire ice volume of the Greenland Ice Sheet would melt, this would result in an overall oceanic uptake of 5.4 Pg of atmospheric CO₂, which hence represents a weak negative feedback to climate change.**

Acknowledgements. This research was supported by the Research Foundation Flanders (FWO aspirant grant to L. Meire) and the Department for Education, Church, Culture and Equality (IIKNN Greenland). D. H. Søgaard was financially supported by the Commission for Scientific Research in Greenland (KVUG). J. Mortensen was financially supported by DEFROST under Nordic Centers of Excellence (NCoE) program. F. J. R. Meysman was financially supported by the Netherlands Orga-

nization for Scientific Research (ZKO project on Coastal Acidification) and the European Research Council (ERC Starting grant 306933). S. Rysgaard was funded by the Canada Excellence Research Chair program. We thank Asiaq (Greenland Survey) for supplying the irradiance data. This study was conducted in collaboration with the marine monitoring program MarineBasis-Nuuk, part of the Greenland Ecosystem Monitoring (GEM). This work is a contribution to the Arctic Science Partnership (ASP) and the ArcticNet Networks of Centers of Excellence programs. We would like to thank Flemming Heinrich, Maia Olsen, Thomas Krogh and the crew of RV *SANNA* for field and laboratory assistance.

References

- Akima, H., Gebhardt, A., Petzoldt, T., and Maechler, M.: Akima: Interpolation of Irregularly Spaced Data, R Packag. version 0.5–1, available at: <http://cran.r-project.org/web/packages/akima> (last access: 14 December 2014), 2006.
- Arendt, K. E., Juul-Pedersen, T., Mortensen, J., Blicher, M. E., and Rysgaard, S.: A 5 year study of seasonal patterns in mesozooplankton community structure in a sub-Arctic fjord reveals dominance of *Microsetella norvegica* (Crustacea, Copepoda), *J. Plankton Res.*, 35, 105–120, doi:10.1093/plankt/fbs087, 2013.
- Bates, N. R. and Mathis, J. T.: The Arctic Ocean marine carbon cycle: evaluation of air-sea CO₂ exchanges, ocean acidification impacts and potential feedbacks, *Biogeosciences*, 6, 2433–2459, doi:10.5194/bg-6-2433-2009, 2009.
- Chen, C.-T. A., Huang, T.-H., Chen, Y.-C., Bai, Y., He, X., and Kang, Y.: Air–sea exchanges of CO₂ in the world’s coastal seas, *Biogeosciences*, 10, 6509–6544, doi:10.5194/bg-10-6509-2013, 2013.
- Delille, B., Jourdain, B., Borges, A.V., Tison, J.-L., and Delille, D.: Biogas (CO₂, O₂, dimethylsulfide) dynamics in Spring Antarctic fast ice, *Limnology and Oceanography*, 52(4), 1367–1379., 2007
- Dickson, A. and Goyet, C.: Handbook of Methods for the Analysis of the Various Parameters of the Carbon Dioxide System in Sea Water, available at: http://cdiac.esd.ornl.gov/oceans/DOE_94.pdf (Accessed 2 September 2014), 1992.
- Dickson, A. G., Sabine, C. L., and Christian, J. R. (Eds.): Guide to best practices for ocean CO₂ measurements, PICES Special Publication 3, 191 pp., 2007.
- Evans, W., Mathis, J. T., and Cross, J. N.: Calcium carbonate corrosivity in an Alaskan inland sea, *Biogeosciences*, 11, 365–379, doi:10.5194/bg-11-365-2014, 2014.

- Fietzek, P., Fiedler, B., Steinhoff, T. and Körtzinger, A.: In situ quality assessment of a novel under-water $p\text{CO}_2$ sensor based on membrane equilibration and NDIR spectrometry, *Journal of Atmospheric and Oceanic Technology*, 31, 181–196, 2014.
- Fuhrman, J. A. and Azam, F.: Thymidine incorporation as a measure of heterotrophic bacterioplankton production in marine surface waters: evaluation and field results, *Mar. Biol.*, 66, 109–120, doi:10.1007/BF00397184, 1982.
- Hastie, T. J. and Tibshirani, R.: *Generalized Additive Models*, Chapman and Hall, London, 1990.
- Hofmann, A. F., Meysman, F. J. R., Soetaert, K., and Middelburg, J. J.: A step-by-step procedure for pH model construction in aquatic systems, *Biogeosciences*, 5, 227–251, doi:10.5194/bg-5-227-2008, 2008.
- Hofmann, A. F., Soetaert, K., Middelburg, J. J., and Meysman, F. J. R.: AquaEnv: an aquatic acid-base modelling environment in R, *Aquat. Geochem.*, 16, 507–546, doi:10.1007/s10498-009-9084-1, 2010.
- Jensen, H. M., Pedersen, L., Burmeister, A., and Hansen, B. W.: Pelagic primary production during summer along 65 to 72° N off West Greenland, *Polar Biol.*, 21, 269–278, doi:10.1007/s003000050362, 1999.
- Juul-Pedersen, T., Arendt, K., Mortensen, J., Blicher, M., Søgaard, D., and Rysgaard, S.: Seasonal and interannual phytoplankton production in a sub-arctic tidewater outlet glacier fjord, west Greenland, *MEPS*, doi: 10.3354/meps11174, 2015.
- Kaltin, S. and Anderson, L. G.: Uptake of atmospheric carbon dioxide in Arctic shelf seas: evaluation of the relative importance of processes that influence $p\text{CO}_2$ in water transported over the Bering–Chukchi Sea shelf, *Mar. Chem.*, 94, 67–79, doi:10.1016/j.marchem.2004.07.010, 2005.
- Langen, P. L., Mottram, R. H., Christensen, J. H., Boberg, F., Rodehacke, C. B., Stendel, M., Van As, D., Ahlstrøm, A. P., Mortensen, J., Rysgaard, S., Petersen, D., Svendsen, K. H., Aðalgeirsdóttir, G., and Cappelen, J.: Recent changes in energy and freshwater budgets for the Godthåbsfjord catchment simulated in a 5 km regional climate model, *J. Climate*, 2014.
- Mathis, J. T., Cross, J. N., and Bates, N. R.: Coupling primary production and terrestrial runoff to ocean acidification and carbonate mineral suppression in the eastern Bering Sea, *J. Geophys. Res.*, 116, 2156–2202, doi:10.1029/2010JC006453, 2011.
- Mook, W. G. and Koene, B. K. S.: Chemistry of dissolved inorganic carbon in estuarine and coastal brackish waters, *Estuar. Coast. Mar. Sci.*, 3, 325–336, doi:10.1016/0302-3524(75)90032-8, 1975.

- Mortensen, J., Lennert, K., Bendtsen, J., and Rysgaard, S.: Heat sources for glacial melt in a sub-Arctic fjord (Godthåbsfjord) in contact with the Greenland Ice Sheet, *J. Geophys. Res.*, 116, 1–13, doi:10.1029/2010JC006528, 2011.
- Mortensen, J., Bendtsen, J., Motyka, R. J., Lennert, K., Truffer, M., Fahnestock, M., and Rysgaard, S.: On the seasonal freshwater stratification in the proximity of fast-flowing tide-water outlet glaciers in a sub-Arctic sill fjord, *J. Geophys. Res.-Ocean.*, 118, 1382–1395, doi:10.1002/jgrc.20134, 2013.
- Nakaoka, S.-I., Aoki, S., Nakazawa, T., Hashida, G., Morimoto, S., Yamanouchi, T., and Inoue, H. Y.: Temporal and spatial variations of oceanic $p\text{CO}_2$ and air–sea CO_2 flux in the Greenland Sea and the Barents Sea, *Tellus B*, 58, 148–161, doi:10.1111/j.1600-0889.2006.00178.x, 2006.
- Nielsen, E. S.: The use of radio-active carbon (C^{14}) for measuring organic production in the sea, *J. Conseil.*, 18, 117–140, 1952.
- Nightingale, P. D., Malin, G., Law, C. S., Watson, A. J., Liss, P. S., Liddicoat, M. I., Boutin, J., and Upstill-Goddard, R. C.: In situ evaluation of air–sea gas exchange parameterizations using novel conservative and volatile tracers, *Global Biogeochem. Cy.*, 14, 373–387, doi:10.1029/1999GB900091, 2000.
- R Core Team: R Development Core Team, *R A Lang. Environ. Stat. Comput.*, available at: <http://www.R-project.org>, 2013.
- Reisdorph, S. C. and Mathis, J. T.: The dynamic controls on carbonate mineral saturation states and ocean acidification in a glacially dominated estuary, *Estuar. Coast. Shelf S.*, 144, 8–18, doi:10.1016/j.ecss.2014.03.018, 2014.
- Rignot, E., Velicogna, I., Van Den Broeke, M. R., Monaghan, A., and Lenaerts, J.: Acceleration of the contribution of the Greenland and Antarctic ice sheets to sea level rise, *Geophys. Res. Lett.*, 38, L05503, doi:10.1029/2011GL046583, 2011.
- Rivkin, R. B. and Legendre, L.: Biogenic carbon cycling in the upper ocean: effects of microbial respiration, *Science*, 291, 2398–400, doi:10.1126/science.291.5512.2398, 2001.
- Rysgaard, S., Mortensen, J., Juul-Pedersen, T., Sørensen, L. L., Lennert, K., Søgaard, D. H., Arendt, K. E., Blicher, M. E., Sejr, M. K., and Bendtsen, J.: High air–sea CO_2 uptake rates in nearshore and shelf areas of Southern Greenland: temporal and spatial variability, *Mar. Chem.*, 128–129, 26–33, doi:10.1016/j.marchem.2011.11.002, 2012.
- Sejr, M. K., Krause-Jensen, D., Rysgaard, S., Sørensen, L. L., Christensen, P. B., and Glud, R. N.: Air–sea flux of CO_2 in arctic coastal waters influenced by glacial melt water and sea ice, *Tellus B*, 63, 815–822, doi:10.1111/j.1600-0889.2011.00540.x, 2011.

- Sejr, M. K., Krause-Jensen, D., Dalsgaard, T., Ruiz-Halpern, S., Duarte, C. M., Middelboe, M., Glud, R. N., Bendtsen, J., Balsby, T. J. S., and Rysgaard, S.: Seasonal dynamics of autotrophic and heterotrophic plankton metabolism and PCO_2 in a subarctic Greenland fjord, *Limnol. Oceanogr.*, 59, 1764–1778, doi:10.4319/lo.2014.59.5.1764, 2014.
- Shadwick, E. H., Thomas, H., Azetsu-Scott, K., Greenan, B. J. W., Head, E., and Horne, E.: Seasonal variability of dissolved inorganic carbon and surface water $p\text{CO}_2$ in the Scotian Shelf region of the Northwestern Atlantic, *Mar. Chem.*, 124, 23–37, doi:10.1016/j.marchem.2010.11.004, 2011.
- Soetaert, K. and Meysman, F.: Reactive transport in aquatic ecosystems: rapid model prototyping in the open source software R, *Environ. Modell. Softw.*, 32, 49–60, doi:10.1016/j.envsoft.2011.08.011, 2012.
- Soetaert, K., Petzoldt, T., and Setzer, R. W.: Package deSolve: solving initial value differential equations in R, *J. Stat. Softw.*, 33, 1–25, available at: <http://www.jstatsoft.org/v33/i09/paper> (last access: 14 December 2014), 2010.
- Søgaard, D., Kristensen, M., Rysgaard, S., Glud, R., Hansen, P., and Hilligsøe, K.: Autotrophic and heterotrophic activity in Arctic first-year sea ice: seasonal study from Malene Bight, SW Greenland, *Mar. Ecol.-Prog. Ser.*, 419, 31–45, doi:10.3354/meps08845, 2010.
- Takahashi, T., Sutherland, S. C., Sweeney, C., Poisson, A., Metzl, N., Tilbrook, B., Bates, N., Wanninkhof, R., Feely, R. A., Sabine, C., Olafsson, J., and Nojiri, Y.: Global sea–air CO_2 flux based on climatological surface ocean $p\text{CO}_2$, and seasonal biological and temperature effects, *Deep-Sea Res. Pt. II*, 49, 1601–1622, doi:10.1016/S0967-0645(02)00003-6, 2002.
- Thomas, H. and Schneider, B.: The seasonal cycle of carbon dioxide in Baltic Sea surface waters, *J. Marine Syst.*, 22, 53–67, doi:10.1016/S0924-7963(99)00030-5, 1999.
- Thomas, H., Bozec, Y., Elkalay, K., and de Baar, H. J. W.: Enhanced open ocean storage of CO_2 from shelf sea pumping, *Science*, 304, 1005–1008, doi:10.1126/science.1103193, 2004.
- Torres, R., Pantoja, S., Harada, N., González, H. E., Daneri, G., Frangopulos, M., Rutllant, J. A., Duarte, C. M., Rúa-Halpern, S., Mayol, E., and Fukasawa, M.: Air–sea CO_2 fluxes along the coast of Chile: from CO_2 outgassing in central northern upwelling waters to CO_2 uptake in southern Patagonian fjords, *J. Geophys. Res.*, 116, C09006, doi:10.1029/2010JC006344, 2011.
- Van As, D., Andersen, M. L., Petersen, D., Fettweis, X., Van Angelen, J. H., Lenaerts, J. T. M., Van Den Broeke, M. R., Lea, J. M., Bøggild, C. E., Ahlstrøm, A. P., and Steffen, K.: Increasing meltwater discharge from the Nuuk region of the Greenland ice sheet and implications for mass balance (1960–2012), *J. Glaciol.*, 60, 314–322, doi:10.3189/2014JoG13J065, 2014.

- Wanninkhof, R.: Relationship between gas exchange and wind speed over the ocean, *J. Geophys. Res.*, 97, 7373–7381, 1992.
- Wanninkhof, R. and McGillis, W. R.: A cubic relationship between air–sea CO₂ exchange and wind speed, *Geophys. Res. Lett.*, 26, 1889–1892, doi:10.1029/1999GL900363, 1999.
- Whitfield, M. and Turner, D.: The carbon dioxide system in estuaries-an inorganic perspective, *Sci. Total Environ.*, 49, 235–255, available at: <http://www.sciencedirect.com/science/article/pii/0048969786902433> (last access: 23 September 2014), 1986.
- Wolf-Gladrow, D. A., Zeebe, R. E., Klaas, C., Körtzinger, A., and Dickson, A. G.: Total alkalinity: the explicit conservative expression and its application to biogeochemical processes, *Mar. Chem.*, 106, 287–300, doi:10.1016/j.marchem.2007.01.006, 2007.

Table 1. Mass balance equations of the biogeochemical model. V_i and A_i are respectively the volumes and areas of the different zones. $\Delta p\text{CO}_2$ is the difference in $p\text{CO}_2$ of the water (modelled) and the atmospheric $p\text{CO}_2$ (400 μatm) with negative values implying an uptake by the sea. α is the CO_2 solubility ($\text{mol m}^{-3} \text{atm}^{-1}$). K_{av} (m s^{-1}) is the gas transfer coefficient calculated using the formulation of Nightingale et al. (2000). NCP is the net community production. [The glacial meltwater input into the fjord \$Q_g\(t\)\$ is imposed as a forcing function upon the model - see material and methods for details how \$Q_g\(t\)\$ is parameterized as a function of time.](#)

Water mass balance	
Zone 1: $Q_1(t) = Q_2(t) + F_1(t)$	1
Zone 2: $Q_2(t) = Q_3(t) + F_2(t)$	2
Zone 3: $Q_3(t) = Q_g(t) + F_3(t)$	3
Salinity mass balance	
Zone 1: $\frac{dS_1}{dt} = \frac{1}{V_1} (Q_2(t)S_2 + F_1(t)S_{\text{SW}} - Q_1(t)S_1)$	4
Zone 2: $\frac{dS_2}{dt} = \frac{1}{V_2} (Q_3(t)S_3 + F_2(t)S_{\text{SW}} - Q_2(t)S_2)$	5
Zone 3: $\frac{dS_3}{dt} = \frac{1}{V_3} (Q_g(t)S_{\text{FW}} + F_3(t)S_{\text{SW}} - Q_3(t)S_3)$	6
Total alkalinity (TA) mass balance	
Zone 1: $\frac{d\text{TA}_1}{dt} = \frac{1}{V_1} (Q_2(t)\text{TA}_2 + F_1(t)\text{TA}_{\text{SW}} - Q_1(t)\text{TA}_1)$	7
Zone 2: $\frac{d\text{TA}_2}{dt} = \frac{1}{V_2} (Q_3(t)\text{TA}_3 + F_2(t)\text{TA}_{\text{SW}} - Q_2(t)\text{TA}_2)$	8
Zone 3: $\frac{d\text{TA}_3}{dt} = \frac{1}{V_3} (Q_g(t)\text{TA}_{\text{FW}} + F_3(t)\text{TA}_{\text{SW}} - Q_3(t)\text{TA}_3)$	9
Dissolved inorganic carbon (DIC) balance	
Zone 1: $\frac{d\text{DIC}_1}{dt} = \frac{1}{V_1} (Q_2(t)\text{DIC}_2 + F_1(t)\text{DIC}_{\text{SW}} - Q_1(t)\text{DIC}_1) - \frac{A_1}{V_1} K_{\text{av}} \alpha \Delta p\text{CO}_2(t) - \text{NCP}_1(t)$	10
Zone 2: $\frac{d\text{DIC}_2}{dt} = \frac{1}{V_2} (Q_3(t)\text{DIC}_3 + F_2(t)\text{DIC}_{\text{SW}} - Q_2(t)\text{DIC}_2) - \frac{A_2}{V_2} K_{\text{av}} \alpha \Delta p\text{CO}_2(t) - \text{NCP}_2(t)$	11
Zone 3: $\frac{d\text{DIC}_3}{dt} = \frac{1}{V_3} (Q_g(t)\text{DIC}_{\text{FW}} + F_3(t)\text{DIC}_{\text{SW}} - Q_3(t)\text{DIC}_3) - \frac{A_3}{V_3} K_{\text{av}} \alpha \Delta p\text{CO}_2(t) - \text{NCP}_3(t)$	12

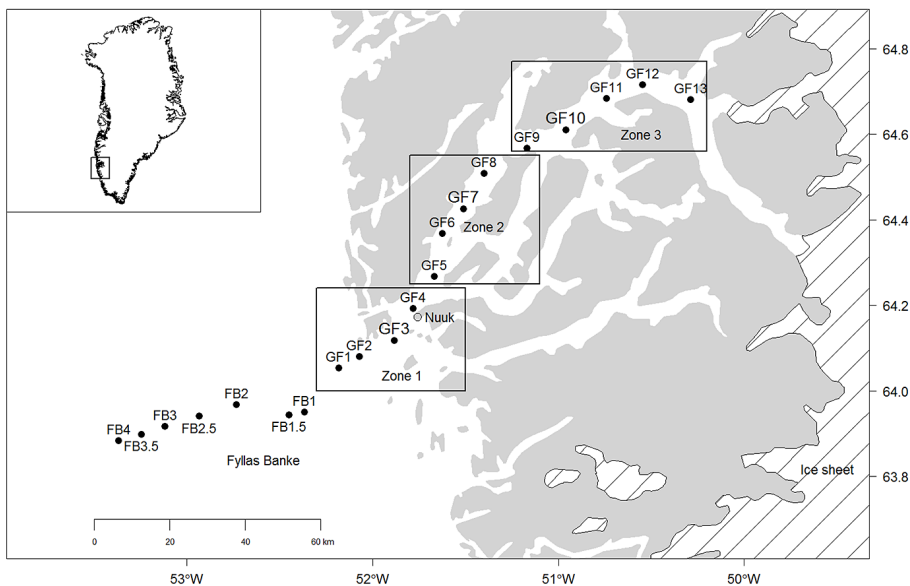


Figure 1. Map of the Godthåbsfjord system with the sampling stations in the fjord system and at Fyllas Banke (SW Greenland). The fjord system is divided in 3 zones indicated by a box. Meteorological data is available from a station in Nuuk.

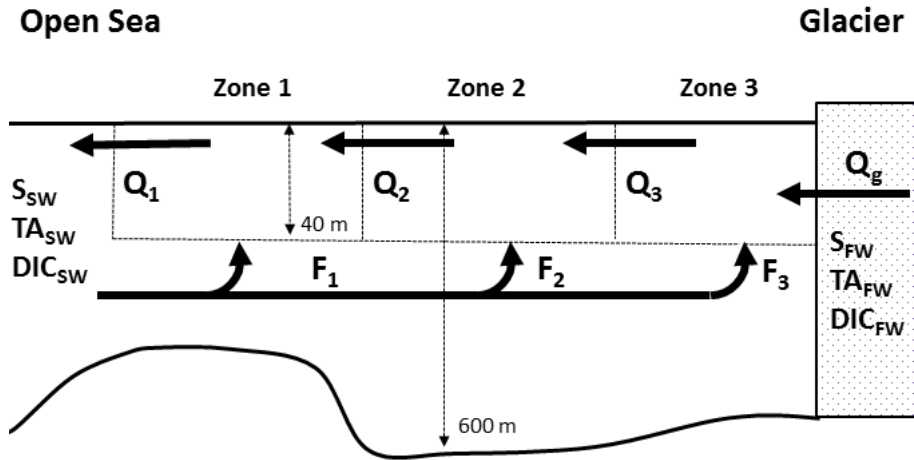


Figure 2. Conceptual model of the fjord system from glacier (right) to open sea (left). The fjord is divided in 3 zones (according to the zones indicated on the overview map).

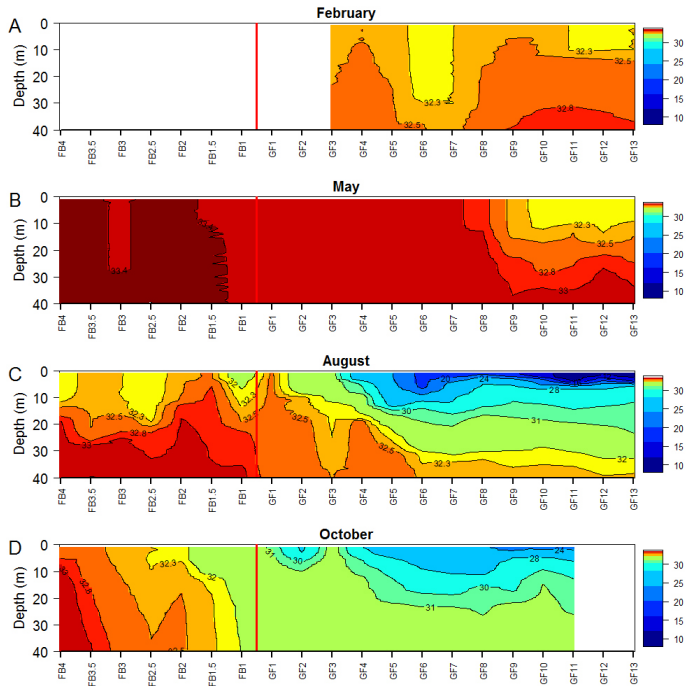


Figure 3. Transects of salinity from shelf (left) to the glaciers (right) during February (a), May (b), August (c) and October (d) 2013. The red line indicates the mouth of Godthåbsfjord area.

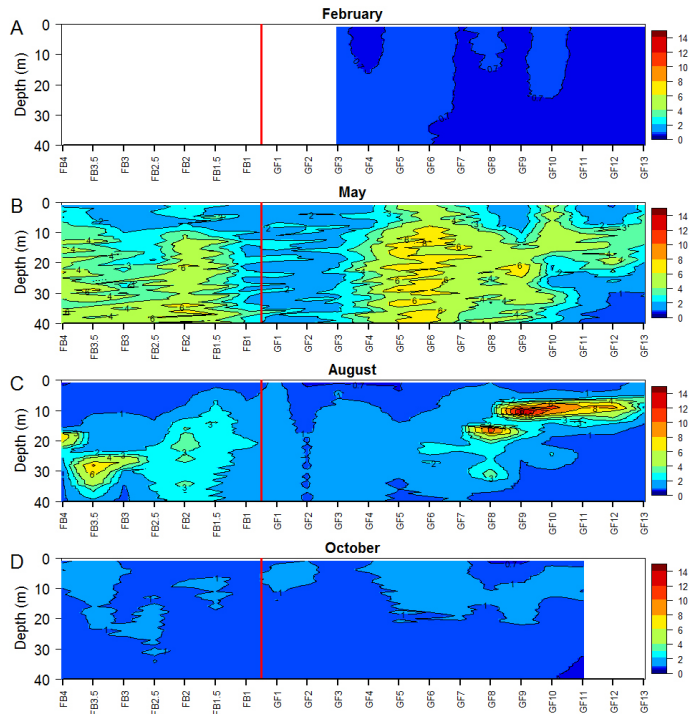


Figure 4. Transects of fluorescence (calibrated vs. chlorophyll a in $\mu\text{g L}^{-1}$) from shelf area (left) to glaciers (right) during February (a), May (b), August (c) and October (d) 2013. The red line indicates the mouth of Godthåbsfjord area.

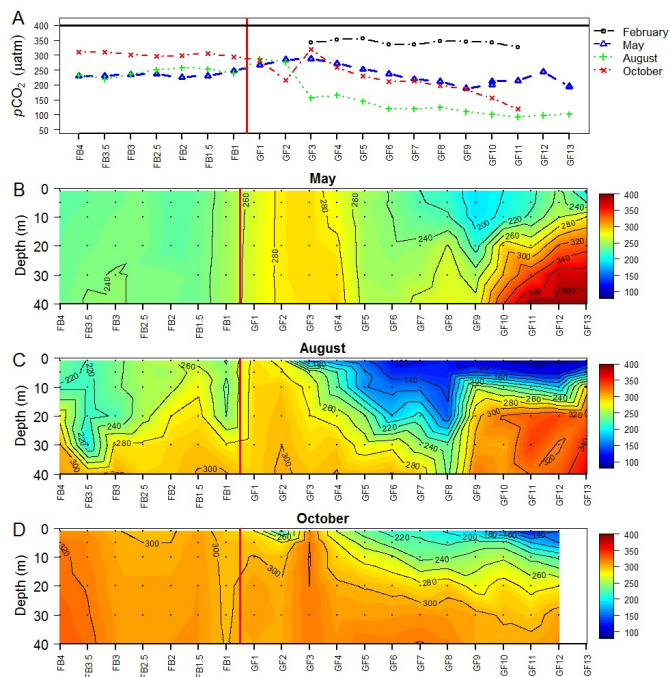


Figure 5. Partial CO₂ pressure data ($p\text{CO}_2$ in μatm) at 1 m depth for the four cruises (a). The full line indicates the average atmospheric concentration (400 μatm) measured during the year 2013. $p\text{CO}_2$ data for the May (b), August (c) and October (d) cruise in the upper 40 m water column from shelf area (left) to glaciers (right). The red line indicates the mouth of Godthåbsfjord area.

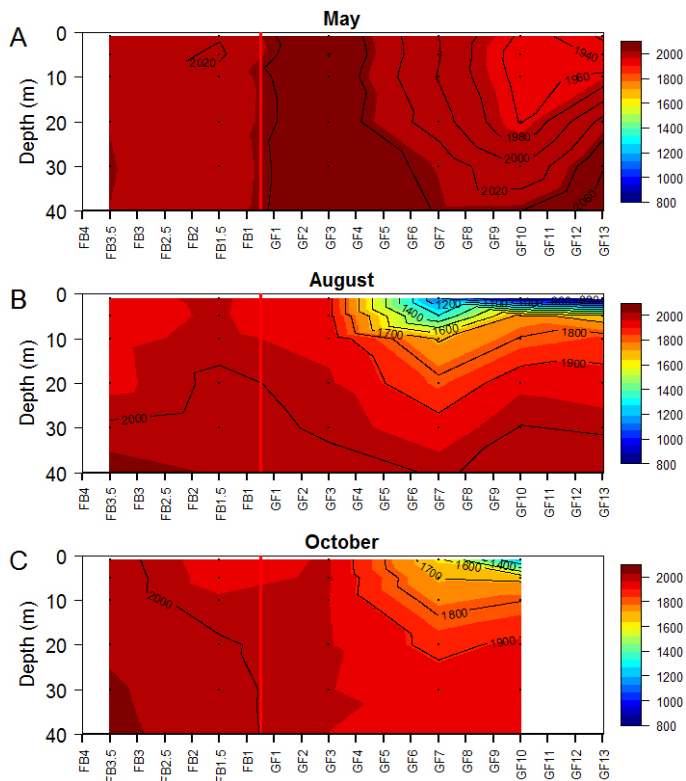


Figure 6. Dissolved inorganic carbon (DIC in $\mu\text{mol kg}^{-1}$) data for May (a), August (b) and October (c) 2013 along a transect from the shelf (left) to the glaciers (right). The red line indicates the mouth of Godthåbsfjord area.

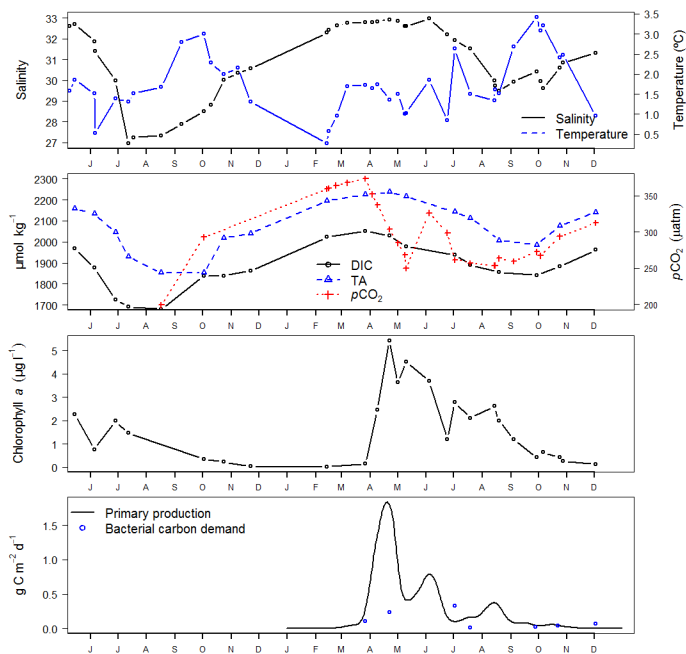


Figure 7. Time series of average (0–40 m) salinity and temperature ($^{\circ}\text{C}$) **(a)**, DIC, TA ($\mu\text{mol kg}^{-1}$) and CO_2 partial pressure ($p\text{CO}_2$, μatm) **(b)** chlorophyll a concentration ($\mu\text{g L}^{-1}$) **(c)** and primary production and bacterial carbon demand ($\text{g C m}^{-2} \text{d}^{-1}$) **(d)** from June 2012 to December 2013 for station GF10.

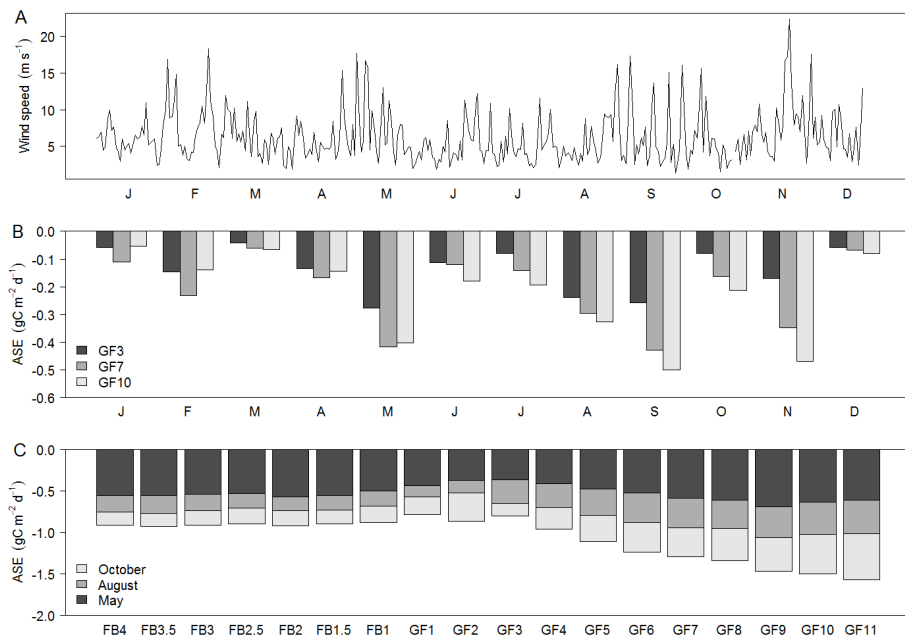


Figure 8. (a) Mean daily wind speed (m s^{-1}) at the meteorological station in Nuuk. (b) Time series of mean monthly air–sea CO_2 flux (ASE, $\text{g C m}^{-2} \text{d}^{-1}$) at three stations (GF3, GF7 and GF10) in the fjord. (c) Mean air–sea exchange (ASE, $\text{g C m}^{-2} \text{d}^{-1}$) from 3 cruises in fjord system from shelf (Fyllas Banke, left) to inner fjord glaciers (right).

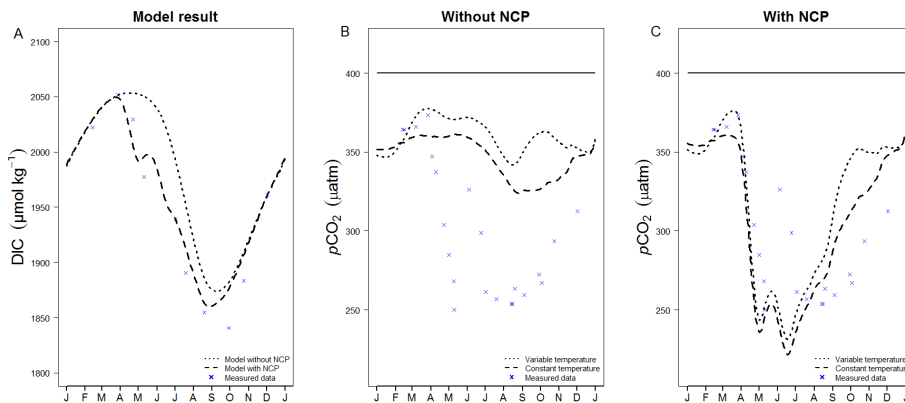


Figure 9. Seasonal evolution of DIC in $\mu\text{mol kg}^{-1}$ (a) and $p\text{CO}_2$ in μatm (b and c) calculated by the biogeochemical model together with data from 2013 in station GF10 (blue points indicate measured data averaged over a 40 m box). Simulations of the model are shown with and without net community production (NCP). Simulations of the evolution of $p\text{CO}_2$ are shown without (b) and with NCP (c) and for a variable temperature and constant temperature (0.5°C , the average winter temperature).

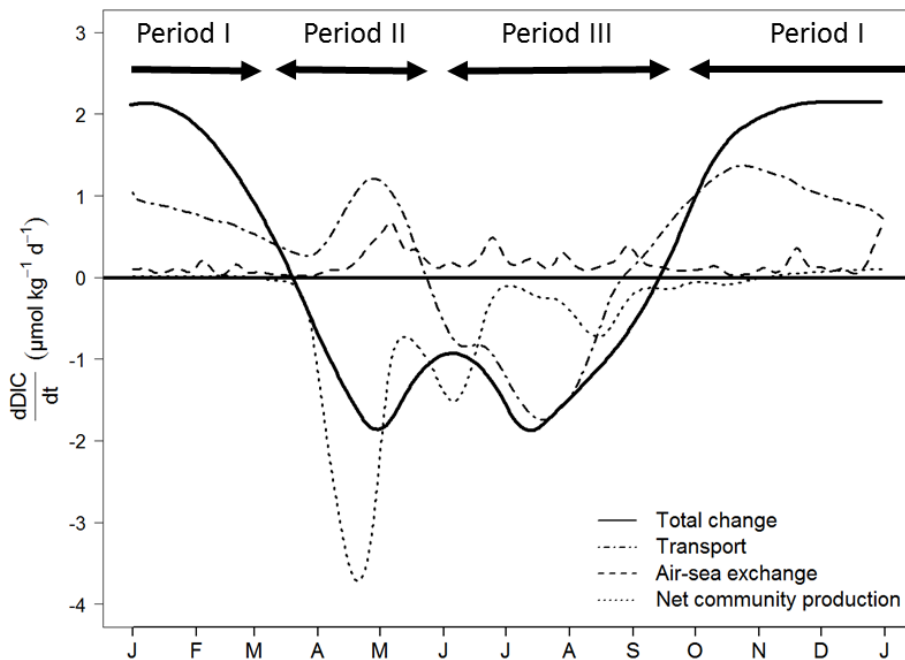


Figure 10. Overview of how different processes (Transport, Air–sea exchange and Net community production) contribute to the temporal observed change in DIC ($\mu\text{mol kg}^{-1} \text{d}^{-1}$) for the station close to the ice sheet (GF10). Uptake of CO_2 by the sea from the atmosphere is shown as a positive value.

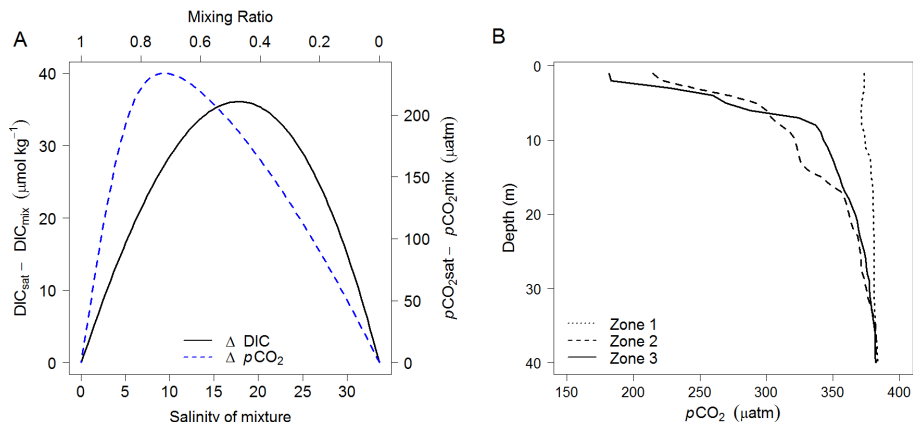


Figure 11. Undersaturation created as ΔDIC (in $\mu\text{mol kg}^{-1}$) and $\Delta p\text{CO}_2$ (in μatm) as a function of salinity of the mixture (and mixing ratio, x , indicating the fraction freshwater) when two water masses in equilibrium with atmosphere are mixed (a). A first water parcel in equilibrium with the atmosphere with TA of $50 \mu\text{mol kg}^{-1}$, DIC of $81.2 \mu\text{mol kg}^{-1}$, salinity of 0 and temperature of 0°C (glacial origin). And a second parcel in equilibrium with the atmosphere with TA of $2220 \mu\text{mol kg}^{-1}$, DIC of $2118 \mu\text{mol kg}^{-1}$, salinity of 33.65 and temperature of 0°C (fjord/sea water). Panel (b) shows the estimated $p\text{CO}_2$ profile calculated from the salinity profiles of August in the three different zones in the fjord system.